Mol Neurobiol (2017) 54:3439–3452
DOI 10.1007/s12035-016-9925-z

MicroRNA-338 Attenuates Cortical Neuronal Outgrowth by Modulating the Expression of Axon Guidance Genes

Aron Kos[1,2] · **Teun Klein-Gunnewiek**[1,2] · **Julia Meinhardt**[1,2] · **Nikkie F. M. Olde Loohuis**[1,2] · **Hans van Bokhoven**[1,3,2] · **Barry B. Kaplan**[4] · **Gerard J. Martens**[5,2] · **Sharon M. Kolk**[5,2] · **Armaz Aschrafi**[2,4]

Received: 14 January 2016 / Accepted: 3 May 2016 / Published online: 14 May 2016

Abstract MicroRNAs (miRs) are small non-coding RNAs that confer robustness to gene networks through post-transcriptional gene regulation. Previously, we identified miR-338 as a modulator of axonal outgrowth in sympathetic neurons. In the current study, we examined the role of miR-338 in the development of cortical neurons and uncovered its downstream mRNA targets. Long-term inhibition of miR-338 during neuronal differentiation resulted in reduced dendritic complexity and altered dendritic spine morphology. Furthermore, monitoring axon outgrowth in cortical cells revealed that miR-338 overexpression decreased, whereas inhibition of miR-338 increased axonal length. To identify gene targets mediating the observed phenotype, we inhibited miR-338 in cortical neurons and performed whole-transcriptome analysis. Pathway analysis revealed that miR-338 modulates a subset of transcripts involved in the axonal guidance machinery by means of direct and indirect gene targeting. Collectively, our results implicate miR-338 as a novel regulator of cortical neuronal maturation by fine-tuning the expression of gene networks governing cortical outgrowth.

Keywords MicroRNA · Cortex · Neurodevelopment · Neurite development · Robo2

Electronic supplementary material The online version of this article (doi:10.1007/s12035-016-9925-z) contains supplementary material, which is available to authorized users.

✉ Armaz Aschrafi
Armaz.aschrafi@nih.gov

[1] Department of Cognitive Neuroscience, Radboud university medical center, 6500 HB Nijmegen, The Netherlands

[2] Donders Institute for Brain, Cognition, and Behaviour, Centre for Neuroscience, 6525 AJ Nijmegen, The Netherlands

[3] Department of Human Genetics, Radboud university medical center, 6500 HB Nijmegen, The Netherlands

[4] Laboratory of Molecular Biology, National Institute of Mental Health, National Institutes of Health, Bethesda, Maryland 20892, USA

[5] Department of Molecular Animal Physiology, Radboud University, Nijmegen, The Netherlands

Introduction

The cerebral cortex is a highly laminated and parcellated brain structure harbouring an intricate network of neuronal circuitries. The correct functioning of the cortex depends on the precise formation of its neural network architecture. In addition, several neurological disorders such as intellectual disability, schizophrenia and epilepsy display distinct alterations in cortical structure and circuitry [1–5]. One critical step in the neurodevelopmental processes which underlie the formation of the cortex, involves the outgrowth of dendrites and axons to form functional cortical networks [6]. Neural network formation is tightly regulated by a set of both intrinsic and extrinsic factors and understanding how these factors are involved in modulating the gene networks during cortical development is key for understanding neurodevelopmental disorders.

MicroRNAs (miRs) have emerged as a class of evolutionarily conserved small non-coding RNAs (ncRNAs) that regulate gene expression post-transcriptionally. Due to their relatively small binding sequence, a single miR can interact with multiple downstream mRNAs, while a single mRNA can be regulated by several miRs, enabling a single miR to convey robustness to an entire gene network with shared physiological roles [7–10]. Due to these assets, miRs represent a particularly vital group of gene network regulators. Importantly, a growing number of experiments have thus far identified a critical role for individual miRs in orchestrating the tightly

regulated gene expression required to direct cortical development. These investigations have shown that the activity of single miRs can be critical in controlling neurodevelopmental aspects such as neurogenesis [11], neuronal migration [12], axon and dendrite development [13, 14], and ultimately synapse formation [15] and neuronal plasticity [16, 17]. Furthermore, a growing body of evidence suggests that even slight aberrations in miR activity can be detrimental to neuronal function [18–20].

Previously, miR-338 has been shown to play a critical role in a number of cell differentiation processes [21, 22]. For example, miR-338 is encoded intronically within its host gene, the apoptosis-associated tyrosine kinase (*AATK*), a gene implicated in neuroblastoma differentiation and the control of axon and dendrite outgrowth in cortical neurons [23–25]. In addition, miR-338 is enriched in the axons of sympathetic neurons [26] and is capable of locally modulating mitochondrial activity by regulating cytochrome c oxidase, subunit IV (COXIV) in the distal parts of axons [27]. Since neurite outgrowth is crucial for regeneration, miR-338 may be of critical importance in the treatment of neurological diseases. Notably, miR-338 was upregulated in blood leukocytes as well as in cerebrospinal fluid, serum, and spinal cord of amyotrophic lateral sclerosis (ALS) patients [28]. Furthermore, its genomic region is frequently altered in neuroblastoma with mRNA targets encoding proteins involved in cell proliferation, neuroblast differentiation, neuroblast migration and apoptosis [29].

While most of the studies on miR-338 have been reported in cells from the peripheral nervous system, miR-338 is known to be broadly expressed in the central nervous system (CNS) including the cortex [30]. Accumulating evidence indicates that this miR and its host gene *AATK* are involved in axonal outgrowth and differentiation [24, 27]. However, little is known about its role in the differentiation and development of cortical neurons. In the present study, we examined the role of miR-338 in acting as a modulator of differentiation of cortical neuronal cells. Collectively, our results reveal the impact of miR-338 on normal cortical neuronal development, and identify miR-338 as a controller of genes within the axon guidance pathway through direct or non-canonical targeting of downstream transcripts. Among these we found Roundabout, axon guidance receptor, homolog 2 (*Robo2*) as one of the direct miR-338 targets. Through collective regulation of these axon guidance genes, we place miR-338 as a vital regulator of dendrite development and axonal growth.

Material and Methods

Animals Embryonic day 18 (E18) embryos from timed-pregnant Wistar rats (Harlan laboratories B.V., Boxmeer, The Netherlands) were used as a resource for the isolation of primary cortical neurons. Animals were housed 2–3 per cage with ad libitum food and water access with a 12 h light cycle at controlled ambient temperature (21 ± 1 °C). All animal use, care and experiments were performed according to protocols approved by the Committee for Animal Experiments of the Radboud University Nijmegen Medical Centre, Nijmegen, The Netherlands.

Cell Culture HEK-293T cells were cultured in Dulbecco's Modified Eagle Medium (DMEM) high glucose (4.5 g/L) (Life Technology, Grand Island, NY) supplemented with 10 % foetal bovine serum (FBS) (Life Technology, Grand Island, NY) and penicillin-streptomycin (Pen/Strep) antibiotic mixture (Life Technology, Grand Island, NY). The cells were maintained at 37 °C and 10 % CO_2. Primary cortical neurons were isolated from E18 rat embryonic brains. The cortical region was isolated and placed in ice-cold Hanks' Balanced Salt solution (HBSS) containing 2 mmol/L GlutaMAX (Life Technology, Grand Island, NY) and Pen/Strep antibiotics. Cortical tissue was washed two times with the HBSS washing buffer before adding a 0.025 % trypsin in HBSS solution followed by incubation at 37 °C for 15 min. After incubation, the tissue was washed three times with the HBSS washing buffer before adding Neurobasal (NB) medium (Life Technology, Grand Island, NY) supplemented with 10 % FBS and 2 mmol/L GlutaMAX. The tissue was titrated several times with a glass Pasteur pipette, this treatment was repeated with a fire-polished tip glass Pasteur pipette to obtain fully dissociated cells. Separated cells were seeded in cell culture plates, which were coated overnight with 0.1 g/L, mol wt 70, 000–150,000 poly-D-lysine (PDL) (Sigma–Aldrich, St. Louis, MO). For the first 5 h, the cells were cultured in medium containing NB medium with 10 % FBS and 2 mmol/L glutaMAX. Afterwards, the medium was replaced with culturing medium containing NB with the serum free neural supplement B27 (Life Technology, Grand Island, NY) and 2 mmol/L glutaMAX. For culturing pure axonal fractions, microfluidic chambers were prepared by firstly ethanol cleaning the chambers. After the chambers were completely dry, they were placed on PDL coated coverglasses (Hecht Assistent, Sondheim von der Rhön, Germany). The chambers were subsequently filled with 100 μL of NB medium containing 10 % FBS and 2 mmol/L GlutaMAX. This was done at least one day before seeding the cells such that any formed bubbles will be removed. A seeding density of 100,000 cells per chamber was used. All neuronal cell preparations were maintained at 37 °C and with 5 % CO_2.

DNA Constructs and Transfection The miR-338-sponge vectors were made by designing DNA oligonucleotides (Sigma–Aldrich, St. Louis, MO) as previously described [16, 31]. miR Sponge sequences were designed to contain four complementary artificial binding sites for miR-338-3p

(Table 1). Presynthesized DNA oligonucleotides were ligated 3′ to the stop codon of the cDNA-encoding eGFP of the lentiviral pFUGW vector (Addgene, Cambridge, MA) using restriction sites *BsrGI* and *EcoRI*. Luciferase vectors containing the 3′ UTRs of putative miR-338 targets were generated by cloning long DNA oligonucleotides (so-called gBlock fragments) (IDT, Leuven, Belgium) (Table 2) between the *SacI* and *SalI* restriction sites of the pmirGLO Dual-Luciferase miRNA target expression vector (Promega, Madison, WI). For Argonaute2 (*Ago2*) pulldown assays the pIRESneo-FLAG/HA Ago2 vector (Addgene, Cambridge, MA) was used (plasmid # 10822, previously described [32]). All DNA constructs were sequenced to validate their correct identity.

Transfection of primary neurons and mammalian cells was performed using the Screenfect A transfection agent (Genaxxon, Ulm, Germany), following the protocol provided by the manufacturer. In brief, Screenfect A together with either the anti-miR-338 (Exiqon, Vedbaek, Denmark), miR-338 mimic (Qiagen, Germantown, MD) or a corresponding non-targeting (NT) scrambled control were diluted in the provided dilution buffer in order to achieve a final concentration of 30–60 nM. The mixture was applied to the adherent primary neurons and left to incubate at 37 °C for no longer than 24 h. For transfection of HEK-293T cells, ±50,000 cells/cm^2 were first trypsinized, mixed with nucleotide/Screenfect A complexes, and after incubating for 20 mins, the cells were seeded on cell culture plates. For lentivirus production HEK-293T cells were transfected using the $CaCl_2$ method. The viral particles were produced and purified as previously described [33]. The purified viral pellets were resuspended in 100 μL calcium- and magnesium-free HBSS. For infecting primary neurons, ±0.5 μL/cm^2 of concentrated virus was added to the cultures. If a lower infection rate was needed the virus was diluted 10–20 times before adding to the primary neuronal cultures.

Luciferase Assay HEK-293T cells were detached using trypsin and transfected with 75 ng Dual-Glo luciferase vector carrying the appropriate gene 3′ UTR together with 30 or 60 nM miR-338 mimic, anti-miR-338 or a NT control. After addition of the transfection mixture the cells were seeded in 96-well plates. Twenty-four hours after transfection, the cells were used for detection of the luciferase bioluminescence using the Dual-Glo luciferase assay system (Promega, Madison, WI) according to the provided protocol and as previously described [34]. The cells and all the reagents were placed at room temperature to ensure a stable luciferase signal before measuring. For bioluminescence detection, a Victor2 multilabel plate reader (Perkin Elmer, Waltham, MA) was used. Luciferase data was normalized by measurement of renilla luminescence activity (encoded within the pmirGLO Dual-Luciferase miRNA target expression vector) by addition of the Dual-Glo Stop & Glo reagent.

RNA Isolation, Reverse Transcription and Real-Time PCR Total RNA from primary neurons was isolated using the miRNAeasy kit (Qiagen, Germantown, MD), according to the manufacturer's manual which allows for the preservation of both the small RNA and mRNA fraction. RNA purity was determined using the Nanodrop ND1000 (Thermo Scientific, Waltham, MA) UV-spectrophotometer. The 260/280 nm ratios were measured and samples with ratios of 2.0 ±0.05 were considered pure. This was followed by RNA integrity assessment with a 1 % agarose gel imaged with the Gel doc XR system (Bio-Rad, Hercules, CA). Samples showing clearly visible S28 and S18 ribosomal RNA bands were considered to be intact. cDNA was synthesized from isolated RNA according to the protocol provided with the revertAid First Strand cDNA Synthesis Kit (Fermentas, Life Technologies, Waltham, MA). To reverse transcribe small RNAs, the miScript reverse transcription kit (Qiagen, Germantown, MD) was used. Following cDNA synthesis, samples were diluted 1/10 with water. Quantitative real-time PCR (QRT-PCR) detection of mRNA transcripts was performed using the SensiFAST SYBR No-ROX kit (Bioline, London, UK) or the miScript SYBR green PCR kit (Qiagen, Germantown, MD) for the detection of mature miRs according to the manufacturer's manual. See Table 3 for the gene-specific primers that were used. Data were normalized to housekeeping genes (β-actin and U6) using GeNorm software [35].

Immunoprecipitation HEK-293T cells were detached and 500,000 cells were transfected with 1 μg pIRESneo-FLAG/HA Ago2 vector together with either 30 nM miR-338 mimic, 30 nM anti-miR-338 or 30 nM of a NT control. The transfected cells were seeded in 6-well culture plates. The Ago2 immunoprecipitation assay was performed largely as described previously [36], with some minor differences. After 2–3 days of culture, cells were lysed at −80 °C for 1 h with 0.5 mL lysis buffer (10 % glycerol, 20 mM Tris (pH 8), 0.2 mM EDTA, 0.5 % NP-40, 0.5 M KCl, 1 mM DTT, supplemented with Complete mini EDTA-free protease inhibitors (Sigma–Aldrich, St. Louis, MO) and 1 u/μL RiboLock RNase

Table 1 pFUGW lentiviral miR-338 sponge oligonucleotides

miR-338-sp-Fw	5′ GTACACAACAAAATGGAGATGCTGGAATCGCAACAAAATGGAGATGCTGGA ATCGCAACAAAATGGAGATGCTGGAATCGCAACAAAATGGAGATGCTGGAG 3′
miR-338-sp-Rv	5′ AATTCTCCAGCATCTCCATTTTGTTGCGATTCCAGCATCTCCATTTTGTTGCG ATTCCAGCATCTCCATTTTGTTGCGATTCCAGCATCTCCATTTTGTTGT 3′

Table 2 3′ UTR gBlock gene fragments from selected genes (5′→3′)

Robo2	GCATCCGAGCTCAGCTCACTCTTTTTAACTCTGTTCATATTATTGTCTGTTCT GATTGGTCTGTTGTACTATATGTGAATTAATGGGCTGTGGTGCCATATATTAA CTTTTAATTGTGTAACTTTTTATGTTTAAATTTTGCACTGCGATTTTATTTGGT GATAAGCACAAATCTCTACTCCTCATGACATGAAGAAAAGATTGAATGTGAA GGGAGTTTTCTGTACTGTAAGTTAGGTTGGATAATGCTGGTGTAACCAATCC AGTTAGATGGTTTTCAGTTGGGGGTGTAGAAATAGGAAGATCGAAGGAATGA TGGTGTTGGCAAAGTCTTCTTGAAACAACAGATATTGAGACAATTTTAAGAAG CAGAAAGATGGATACTATTGACTAAAGCAGGGGTCAAAAGAAGGGGGTTTAA GTCTAGACAGAGTATGTAATAAAGTATGGTGGTAGCAAAGATGTACTAACTT GCTTTAAAAATAGTCGACGGGACT
Robo2 mutant	GCATCCGAGCTCAGCTCACTCTTTTTAACTCTGTTCATATTATTGTCTGTTCT GATTGGTCTGTTGTACTATATGTGAATTAATGGGCTGTGGTGCCATATATTAA CTTTTAATTGTGTAACTTTTTATGTTTAAATTTTGCACTGCGATTTTATTTGGT GATAAGCACAAATCTCTACTCCTCATGACATGAAGAAAAGATTGAATGTGAA GGGAGTTTTCTGTACTGTAAGTTAGGTTGGATATGTAACCAATCC AGTTAGATGGTTTTCAGTTGGGGGTGTAGAAATAGGAAGATCGAAGGAATGA TGGTGTTGGCAAAGTCTTCTTGAAACAACAGATATTGAGACAATTTTAAGAAG CAGAAAGATGGATACTATTGACTAAAGCAGGGGTCAAAAGAAGGGGGTTTAA GTCTAGACAGAGTATGTAATAAAGTATGGTGGTAGCAAAGATGTACTAACTT GCTTTAAAAATAGTCGACGGGACT

inhibitor (Thermo Scientific, Waltham, MA)). Cell lysates were centrifuged for 10 mins at 12,000×*g*. To the supernatant 20 μL anti-Flag M2 agarose beads (Sigma–Aldrich, St. Louis, MO) was added and incubated for 2 h at 4 °C under gentle agitation. The beads were washed 3 times with lysis buffer followed by elution with 1 mg/mL Flag peptide (sequence DYKDDDDK) (Sigma–Aldrich, St. Louis, MO) in 10 % glycerol, 20 mM Tris (pH 8), 0.2 mM EDTA, 0.5 % NP-40, 0.1 M KCl, 1 mM DTT supplemented with protease and RNAase inhibitors. RNA was isolated from the eluate using the miRNAeasy kit as described above. Equal concentrations of RNA were used for cDNA synthesis.

RNA Sequencing and Bioinformatics Analyses RNA sequencing (RNA-seq) was performed on samples obtained from primary cortical neurons transfected with either an anti-miR-338 or a NT scrambled control RNA (Exiqon, Vedbaek, Denmark) at days in vitro (DIV) 2. RNA was isolated at DIV 6 from three separately generated samples and subsequently pooled to generate one sample for each condition. RNA quality was determined by acquiring the ribosomal integrity number (RIN) using a 2100 Bioanalyzer (Agilent Technologies, Santa Clara, CA), revealing a RIN of above 9.0 for all samples. The samples were subsequently processed further by Hudson Alpha Institute for Biotechnology (Huntsville, AL, USA). Sequencing was performed on two separate flow cells with a total of more than 30 million 50 bp reads per sample. The generated sequencing data was mapped, assembled into genes and analysed using the Genesifter genetic analysis software (Geospiza, Perkin Elmer, Seattle, WA). Normalization was based on the total number of mapped reads and the RPKM (reads per kilobase per million mapped reads) expression threshold was set at 10. Gene expression changes would be considered statistically significant with a p value ≤ 0.001 determined with the likelihood ratio test and Benjamini and Hochberg correction for multiple testing. Gene ontology (GO) and clustering analysis was performed on significantly up and downregulated genes using the DAVID database for

Table 3 List of qPCR primers (5′→3′)

Gene	Forward primer	Reverse primer
ROBO2	TCCGAGCTCCTCCACAGTTT	CGGGAAAAGTAGGTTCTGGCT
ROCK2	GACCACAAAAGCACGACTAGCG	TTCTCGGCTTCCAGGAGTAGGT
PAK1	TCCTCTCGGCTATTACCGGC	AGCAGCTACTTCTGCGCTCG
PAK6	GGCTCGACCACAATCTTGC	AATTGAGCTTGTTCTGTGGCA
UNC5C	TTTCTCAGGACTGCCTGGCG	AAAAGTCATCATCTTGAGCGGC
ABLIM3	GGACGAAGCACCTGAGTCCT	TAAGGCGAGTGGACGAACAG
NEGF	CACTCGCTTGCTTACACACT	GGTGGTTACCTTCCACCTCC
U6	GCTTCGGCAGCA CATATA	CGCTTCACGAATTTGCGT
B-Actin	CGTGAAAAGATGACCCAGATCA	AGAGGCATACAGGGACAACACA
miR-338-3p	TCCAGCATCAGTGATTTTGTTG	Universal reverse primer (Exiqon)

functional gene annotation and KEGG pathway mapping [37, 38]. For GO term clustering of the annotated genes a high stringency setting was used. miR-338 binding sites were identified within the 3′ UTR of genes using DIANA-microT v5.0 algorithm [39]. This program combines both conserved and nonconserved binding sites for each target transcript and combines it to calculate a final prediction score. The higher the prediction scores the lower the likelihood for a false positive target. For our analysis we used a threshold of 0.6.

Immunolabelling and Imaging For immunocytochemistry, cells were fixed with warm (37 °C) 4 % PFA and 16 % sucrose in PBS for 30 min. After washing with PBS (3 × 5 min at RT) cells were incubated for 15 min at RT with 50 mM NH_4Cl to quench residual aldehydes. Cells were washed (3 × 5 min at RT), permeabilized with 0.1 % Trixon X-100 for 5 min at RT, incubated with 2 % BSA (ICN Biomedicals Inc., Santa Ana, CA) in PBS for 30 min at RT to block non-specific staining, and were incubated with the primary antibodies in 2 % BSA in PBS. Incubation in primary antibodies was done overnight at 4 °C. Subsequently, cells were washed in 2 % BSA in PBS (3 × 5 min) and incubated in species-specific, Alexa-conjugated secondary antibodies in 2 % BSA in PBS for 30–60 min at RT, washed in 2 % BSA in PBS (3 × 5 min), and washed (3 × 5 min) in PBS containing fluorescent DAPI (Sigma–Aldrich, St. Louis, MO at 1:3000). The coverslips were mounted in Prolong Gold (Invitrogen). Primary antibodies included chicken anti-GFP (Abcam, Cambridge, UK at 1:500), mouse anti-MAP2 (Sigma–Aldrich, St. Louis, MO at 1:1000), rabbit anti-Robo2 (Sigma–Aldrich, St. Louis, MO at 1:500). Secondary antibodies included Alexa488 goat anti-chicken (Molecular Probes, Life Technologies, Grand Island, NY at 1:500), Alexa568 goat anti-mouse (Molecular Probes, 1:500) and Alexa488 goat anti-rabbit (Molecular Probes, Life Technologies, Grand Island, NY at 1:500). Staining of DIV 3 or DIV 6 neurons cultured in microfluidic chambers was done with acti-stain 488 fluorescent phalloidin according to the provided manufacturer's protocol (Cytoskeleton Inc., Denver, CO). The microfluidic chambers were removed before staining. Images from axon chambers were made by capturing multiple higher magnification micrographs followed by matching and stitching together individual images to generate overview panels of large sections from each chamber. Fluorescent images of the neurons and brain slices were obtained using a Leica DMRA fluorescence microscope fitted with a DFC340 FX CCD camera (Leica, Wetzlar, Germany) or a Leica TCS SP2 AOBS Confocal Laser Scanning Microscope (CLSM) (Leica, Wetzlar, Germany).

Western Blot Primary cortical neurons were transfected at DIV 2 with NT control, miR-338 mimic or anti-miR-338 RNA. Cells were homogenized at DIV 6 with ice-cold lysis buffer (50 mM Tris [pH 8.0], 150 mM NaCl, 1 % Triton X-100, and protease inhibitors). Samples were subjected to Western blot analysis and specific bands were detected using rabbit anti-Robo2 (Sigma–Aldrich, St. Louis, MO at 1:1000) and mouse anti-TUBB3 (Covance, Princeton, NJ at 1:4000).

Neuronal Morphology Analysis The fluorescent images were randomized and analysed in a blinded fashion. For Sholl analysis, images of DIV 21 cortical neurons infected at DIV 6 were taken with a Leica DMRA fluorescent microscope using a ×20 optical zoom. One pixel wide concentric circles originating from the somatic centre were placed over fluorescent neurons using ImageJ software. The intersecting dendrites with each circle were quantified. Axons were measured from panels consisting of stitched together images using the ImageJ plugin, NeuronJ [40]. All axons from an entire chamber were measured from the dotted white line depicted in Fig. 3c, d and averaged. For dendritic spine analysis, spines were imaged using a CLSM with an optical zoom of ×63. Secondary dendritic segments, branching of primary dendrites (originating from the soma) were selected for analysis. Neuronstudio software was used to quantify spine density per dendritic segment and determine the spine head length and diameter [41].

Statistical Analysis Quantitative data are presented as the mean ± s.e.m. Non-paired two-tailed Student's *t* test was used to determine significant differences between two groups. One-way ANOVA with Bonferroni's multiple comparison testing was used to analyse significant differences between multiple groups. $p \leq 0.05$ was considered significant.

Results

MiR-338 Affects Dendritic Complexity and Axon Outgrowth in rat Cortical Neurons in Vitro

To investigate the extend of miR-338 to modulate cortical neuronal differentiation, we first examined its expression levels in rat cortical neurons growing in vitro. In a previous study, we have shown that the expression of this miR in developing primary hippocampal neurons is dynamically regulated [34], however, little is known about the developmental pattern of miR-338 expression in cortical neurons. Towards this end, total RNA was isolated from dissociated primary cortical cultures at eight different neuronal maturation time points, namely DIV 0, 1, 3, 6, 10, 14, 18, and 21 (Fig. 1a). qPCR analysis revealed that miR-338 is expressed relatively early at DIV 0 and 1. Two distinct peaks in miR-338 expression levels were detected at DIV 3 and DIV 18, when the level of this miR increased approximately fourfold as compared to

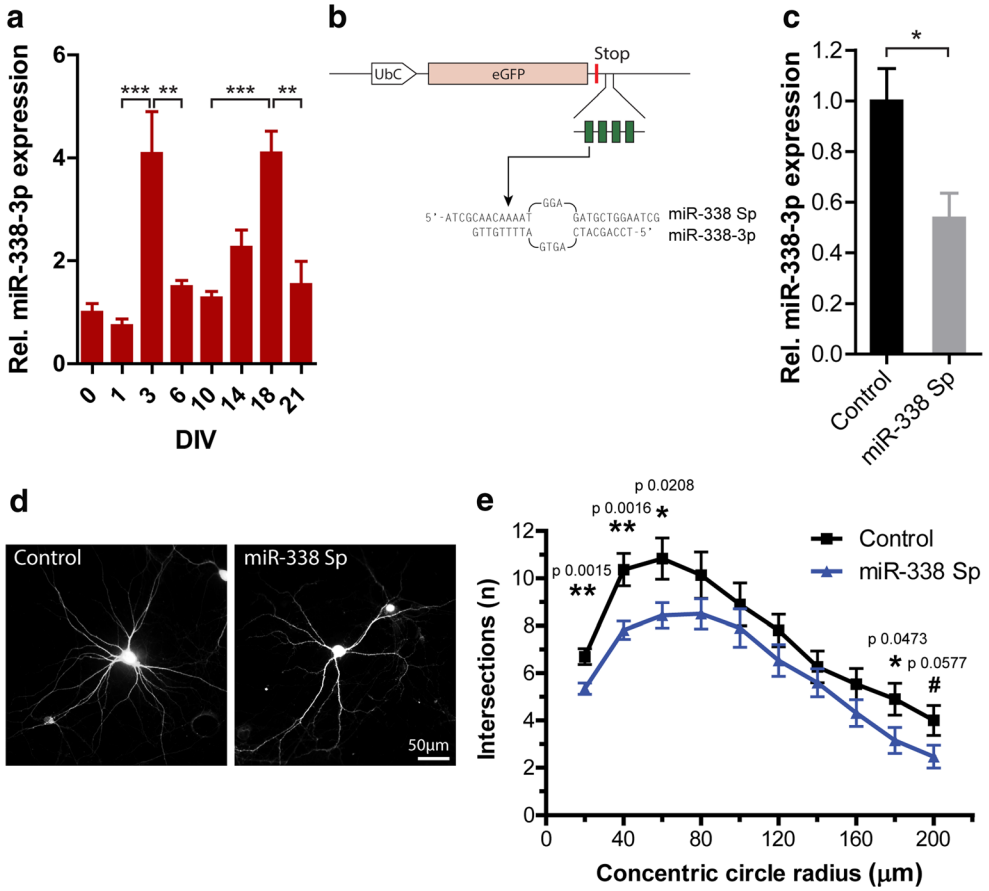

Fig. 1 miR-338 inhibition reduces dendritic complexity in primary rat cortical neurons. **a** Relative expression of miR-338-3p levels determined by qPCR in primary cortical neurons isolated at several developmental time points starting from 0 days in vitro (DIV 0) to DIV 21. Data represents relative fold change as compared to miR-338-3p expression at DIV 0, with *error bars* ± s.e.m. One-way ANOVA with Bonferroni multiple comparison test, $n = 3$ independent experiments with three different samples each; $^{**}p < 0.001$, $^{***}p < 0.0001$. **b** Schematic overview of the miR-338 sponge design to allow for long-term specific sequestering of miR-338-3p. The human ubiquitin c promoter (UbC) promoter driven lentiviral miR-338 sponge construct contains four complementary binding sites for miR-338-3p (highlighted in *green blocks*) within the 3′ UTR the GFP gene. Here, it is also shown how the sponge sequence is designed to interact with the mature miR-338-3p, containing a three-nucleotide bulge to prevent the degradation of the sponge mRNA and an arbitrary four-nucleotide long linker region between each miR-338 binding site. **c** qPCR analysis of miR-338-3p levels of DIV 8 primary cortical neurons infected with a GFP control or the miR-338 sponge at DIV 1. miR-338-3p expression levels were normalized to U6 with the control set to one. Two-tailed unpaired Student's *t* test, $n = 3$ samples from independent experiments; $^{*}p = 0.0282$. **d** Representative micrographs of DIV 21 primary cortical neurons used for the Sholl analysis infected with either control GFP or miR-338-sponge lentivirus at DIV 6. **e** Quantification of dendritic arborisation using Sholl analysis of neurons infected with either control (*black line*) or miR-338 sponge (*blue line*) lentivirus. Data represents the mean with *error bars* ± s.e.m. Two-tailed unpaired Student's *t* test, $n = 30$–33 cells collected from three independent experiments

miR-338 expression at DIV 0. After miR-338 levels peaked, its expression returned to significantly lower levels at DIV 6 and DIV 21 to approximately 1.8-fold of DIV 0 levels. These results suggest that miR-338 is abundantly and dynamically expressed during the growth of cultured cortical neurons. Since these expression peaks correspond to extensive neurite growth and spine development in vitro, we studied whether miR-338 is involved in these processes. We generated a miR-338 repressing (sponge) lentivirus allowing long-term and efficient repression of miR-338 (Fig. 1b). The construct contains four complementary miR-338 sequences within the 3′ UTR of a GFP gene, with each binding site having a central mismatch previously shown to increase the efficiency of miR repression [31, 42]. qPCR analysis of RNAs from primary cortical neurons infected with this miR-338 sponge revealed a significant reduction of miR-338 (Fig. 1c). To test whether endogenous miR-338 has the capacity to modulate dendrite development, we performed the Sholl analysis on mature DIV 21 cortical neurons infected with the miR-338 sponge lentivirus (Fig. 1d, e). Neurons in which miR-338 was inhibited showed a significant decrease in dendritic sprouting (mean 5.344 ± 0.240 versus 6.7 ± 0.333 number of intersections at 20 µm distance from the soma; $p = 0.0015$), as compared to neurons expressing only GFP (Fig. 1e).

Furthermore, cortical neurons infected with a miR-338 sponge exhibited a decrease in dendritic arborisation as revealed by an exacerbated decrease in the number of intersecting dendrites at 40 and 60 μm distance from the soma compared to control-infected neurons. No difference in dendritic complexity was identified in cortical neurons younger than DIV 16 (data not shown), a developmental time point preceding the highest miR-338 expression levels at DIV 18 (Fig. 1a). miR-338's capacity to influence dendrite development led us to analyse the number and morphology of dendritic spines of DIV 21 cortical cells infected with the miR-338 sponge. Morphological analysis of the dendritic spines revealed that miR-338 inhibition failed to alter spine density (mean 0.77 ± 0.06 control vs. 0.75 ± 0.07 miR-338 sponge spines per μm; $p = 0.8254$) (Fig. 2a, b), while it increased spine head diameter (mean 0.52 ± 0.008 control vs. 0.68 ± 0.016 miR-338 sponge μm wide spines; $p = <0.0001$) (Fig. 2c) and spine length (mean 1.287 ± 0.03 control vs. 1.596 ± 0.05 miR-338 sponge μm long spines; $p = <0.0001$) as compared to control GFP-infected neurons (Fig. 2d).

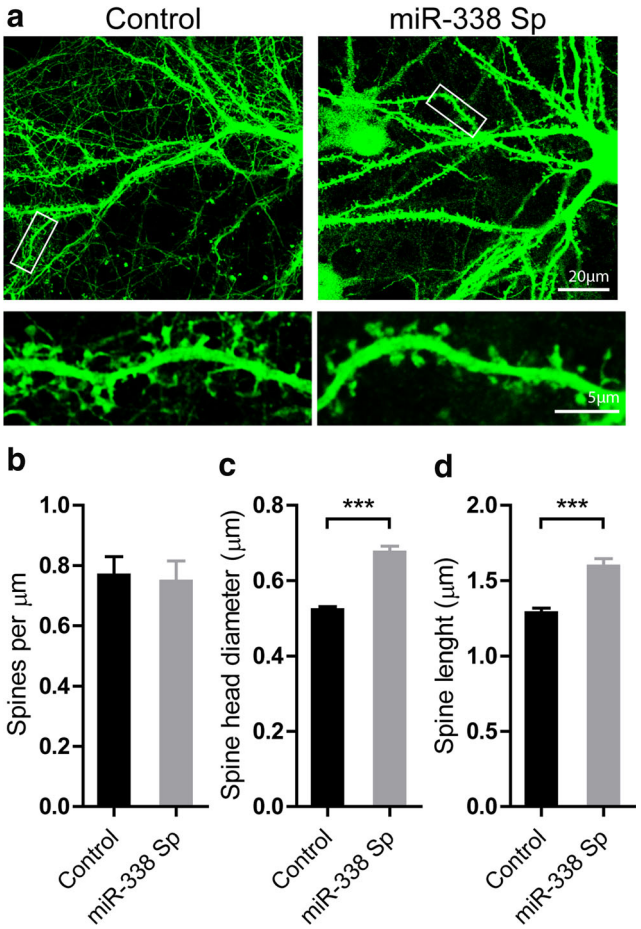

Fig. 2 miR-338 inhibition alters spine morphology in cortical neurons. **a** Images of whole cells (*upper panels*) and high-magnification spiny dendrite images (*lower panels*) of GFP control or miR-338-sponge expressing DIV 21 primary cortical neurons infected at DIV 6. The *inserted boxes* in the upper whole-cell panels represent the magnified areas shown below. Quantifications of **b** average spine density, **c** spine head diameter and **d** spine length are shown for control or miR-338 sponge infected neurons. *Error bars* represent s.e.m. Two-tailed unpaired Student's *t* test, $n = 3$ independent experiments with 8–10 cells per experiment; $^{***}p < 0.0001$

miR-338 was previously observed to attenuate axon growth and function in sympathetic superior cervical ganglia neurons [21]. Furthermore, our qPCR expression study showed that miR-338 has an expression peak in cortical cells after 3 days in culture (Fig. 1a), which coincides with extensive morphological maturation, including increased axon growth and development [43]. To assess the role of miR-338 on axonal outgrowth in cortical cells, we aimed at rapidly and acutely altering miR-338 expression levels in young cortical cells. Since the lentiviral miR-338 sponge acts too slow for sufficient expression inhibition to take place at these earlier time points, we opted to use short miR-338 mimics and anti-miR-338 locked nucleic acid (LNA) oligonucleotides to acutely alter miR-338 levels in developing cortical neurons. In previous studies we revealed that miR-338 mimics and inhibitors are able to significantly increase or decrease miR-338 expression levels within 48–72 h after transfection, respectively [21, 34]. To complement these findings, human embryonic kidney (HEK) 293 cells were transfected with FLAG-tagged Ago2 together with miR-338 mimic or anti-miR-338. Immunoprecipitation of the RNA bound to FLAG-tagged Ago2 2 days after transfection, followed by RNA isolation and qPCR analysis revealed that miR-338 mimic increases whereas anti-miR-338 decreases Ago2 bound miR-338 as compared to a NT scrambled control oligonucleotide (Fig. 3a, b). This finding suggests that transfection of cells with a miR-338 mimic increases; whereas the anti-miR-338 decreases incorporation of mature miR-338 into the RNA induced silencing complex (RISC). To study axon growth in cortical neurons, we used microfluidic chambers, which allowed us to readily trace the extensive network of growing axons [44]. Primary cortical cells were transfected at DIV 2 with miR-338 mimic or anti-miR-338, and after phalloidin staining, axon length was measured at DIV 3 and DIV 6 (Fig. 3c, d). Compared to a NT control, miR-338 overexpressing neurons exhibited an attenuated axon growth at DIV 3 and DIV 6 (mean of 25.5 % decrease at DIV3 and a mean of 39.3 % decrease at DIV6, $p = <0.0001$; Fig. 3e, f), whereas inhibiting miR-338 increased axon outgrowth (mean of 54.2 % increase at DIV 3 and a mean of 31.7 % increase at DIV 6, $p = <0.0001$; Fig. 3e, f). Together, these results emphasize previous observations on the impact of miR-338 alterations on axonal outgrowth in sympathetic superior cervical ganglia neurons [21].

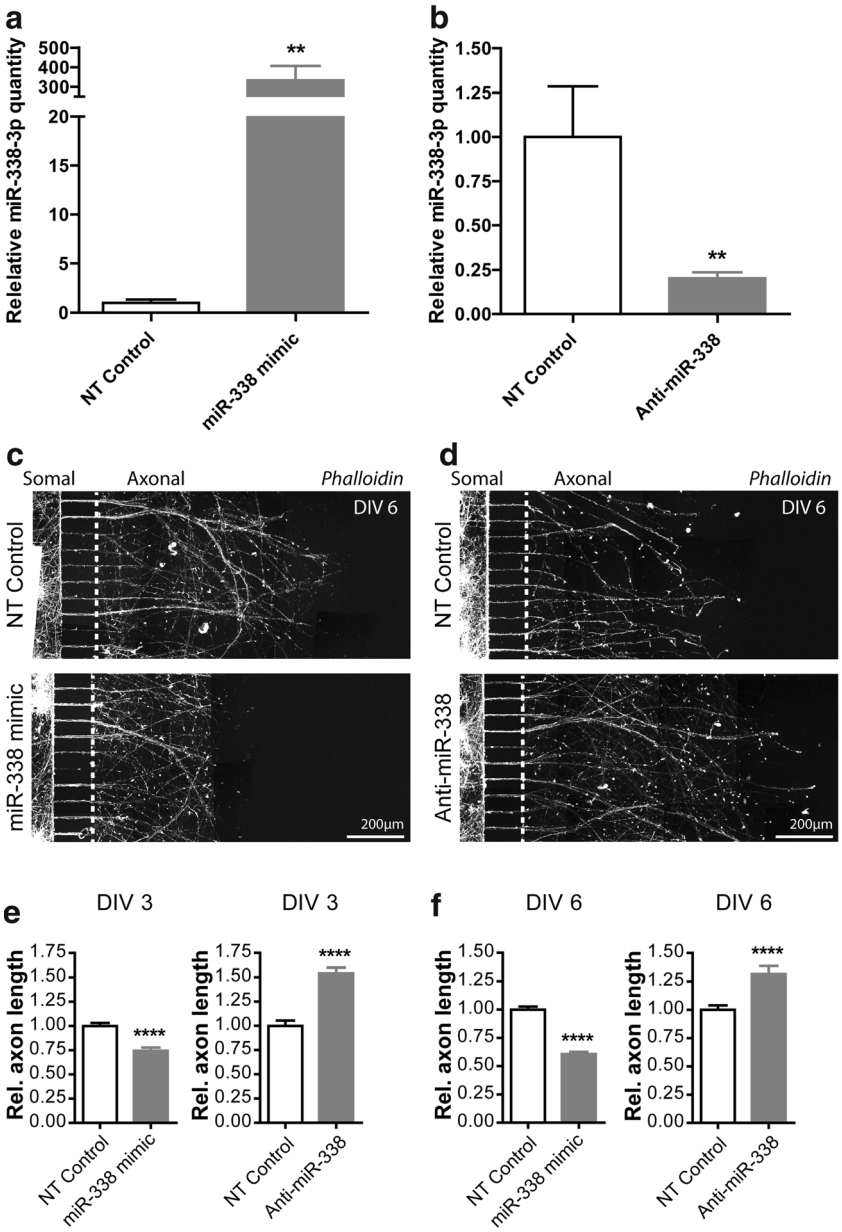

Fig. 3 miR-338 attenuates axonal outgrowth in cultured cortical neurons. **a**, **b** qPCR analysis of miR-338-3p levels in FLAG-tagged Ago2 pull-down samples isolated from HEK-293T cells co-transfected with **a** miR-338 mimic or **b** anti-miR-338 compared to non-targeting (NT) controls. **c**, **d** Representative images of growing axons stained with phalloidin from DIV 6 cortical neurons cultured in microfluidic chambers transfected at DIV 2 with miR-338 mimics, anti-miR-338 or NT controls. Axon bundles were measured from the white dotted line. **e**, **f** Quantified average axonal length of **e** DIV 3 and **f** DIV 6 neurons during overexpression (30 nM miR-338 mimic) or inhibition (30 nM anti-miR-338) of miR-338 relative to a NT-transfected control (30 nM). *Bars* represent mean relative values to control with *error bars* ± s.e.m. Two-tailed unpaired Student's *t* test, axons measured from $n = 3$ chambers per condition; $^{****}p < 0.0001$

miR-338 Regulates the Expression of Axon Guidance Genes

miRs have the capacity to regulate multiple downstream mRNA transcripts, enabling them to refine specific gene networks that control a variety of cellular functions [45, 46]. Previous findings have suggested that regulation by a miR results in mRNA degradation of the vast majority of its target genes [47]. To identify the miR-338 regulated downstream gene networks controlling neuronal development, we performed deep-sequencing of the transcriptome of primary cortical neurons in which miR-338 was inhibited (Fig. 4a). In light of our in vitro neurite outgrowth findings, we opted for the use of DIV 6 primary cortical neurons since there is a high degree of ongoing neurite outgrowth at this time point. To rapidly and acutely inhibit miR-338 function, DIV 2 cortical neurons were transfected with the anti-miR-338. Anti-miR-338-mediated inhibition resulted in the differential expression of 854 genes with 536 downregulated and 318 upregulated transcripts at DIV 6 using a p value cut-off of 0.001 (Fig. 4b). To reveal the corresponding gene networks associated with the inhibition of miR-338, we performed functional gene annotation and clustering analysis using DAVID on the total pool of significantly altered genes. This gene ontology (GO) analysis revealed a large number of miR-338 modulated genes involved in neurite development. The annotation cluster with the highest score (8.64, using a high clustering stringency) consists of six GO terms with the most significant being

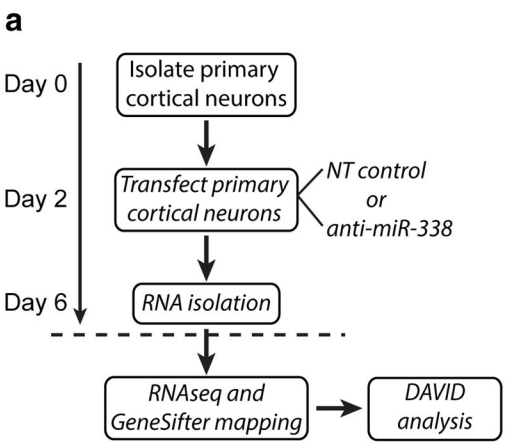

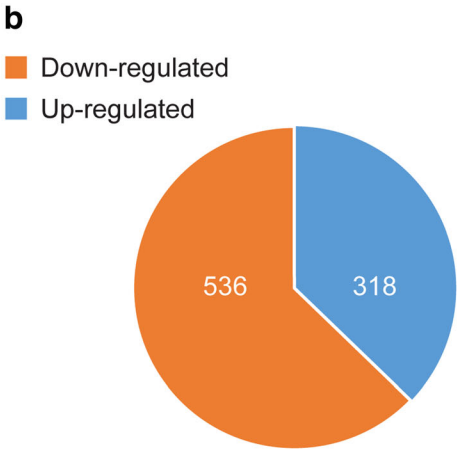

c

GO term annotation clustering on significantly altered transcripts		
Process	**# of molecules**	**p-value**
Neuron projection development	40	3.7E-07
Cell projection organization	47	3.8E-07
Cell part morphogenesis	37	6.2E-07
Neuron projection morphogenesis	34	6.4E-07
Cell projection morphogenesis	36	6.3E-07
Neuron development	45	6.7E-07

d

KEGG pathway analysis on significantly altered transcripts		
Process	**# of molecules**	**p-value**
Axon guidance	17	4.4E-4
Terpenoid backbone biosynthesis	5	3.9E-3
Butanoate metabolism	7	4.8E-3
Pathways in cancer	27	6.6E-3
Valine, leucine and isoleucine degradation	8	6.6E-3
PPAR signaling pathway	10	7.5E-3
Cell cycle	14	8.6E-3
Renal cell carcinoma	9	1.9E-2
Propanoate metabolism	6	2.1E-2
Wnt signaling pathway	14	2.6E-2

e

Symbol	Gene name	Fold change	p-value	Binding site
Dpysl2	Dihydropyrimidinase-like 2	1.05	2.88E-14	
Pak6	P21 (CDKN1A)-activated kinase 6	1.14	4.80E-09	
Robo2	Roundabout, axon guidance receptor, homolog 2 (Drosophila)	1.11	4.93E-09	Y
Unc5c	Unc-5 homolog C (C. elegans)	1.26	9.63E-08	
Ablim3	Actin binding LIM protein family, member 3	1.25	3.95E-06	
Rock2	Rho-associated coiled-coil containing protein kinase 2	1.21	6.68E-06	Y
Ngef	Neuronal guanine nucleotide exchange factor	1.16	2.82E-05	
Pak1	P21 (CDKN1A)-activated kinase 1	1.12	9.36E-05	

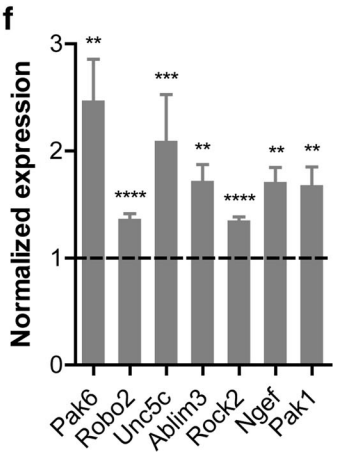

Fig. 4 Transcriptome analysis shows that miR-338 regulates a subset of genes involved in axon growth. **a** An experimental outline of the transcriptome analysis in cortical neurons transfected with anti-miR-338, or NT control oligonucleotides followed by RNA sequencing (RNA-seq) 3 days post transfection. The sequencing data was analysed using DAVID functional annotation and GO term clustering. **b** A pie diagram depicting the number of significantly ($p < 0.001$) upregulated (*blue*) and (*orange*) downregulated genes. **c** Gene ontology based clustering by DAVID showing the annotation cluster with the highest enrichment score (8.64). Presented are the GO term processes, the number of assorted genes clustered within each category and the corresponding p value. **d** Top 10 significant canonical KEGG pathways with the number of associated molecules. **e** A list of significantly upregulated axon guidance genes identified with the KEGG pathway analysis. It shows the gene symbol, full gene name, the fold change increase, the associated p value identified with RNA sequencing and whether or not it has a putative miR-338 binding site identified by DIANA. **f** qPCR validation of the upregulated axon guidance genes identified by RNA sequencing. Data represents the relative to control mean fold change with *error bars* ± s.e.m. Two-tailed unpaired Student's t test, $n = 3$ samples from independent experiments; $^{**}p < 0.01$, $^{***}p < 0.001$ and $^{****}p < 0.0001$

neuron projection development, with a p value of 3.70E-07 (Fig. 4c). This finding suggests that miR-338 has the capacity to control a set of neurodevelopmental genes either by directly binding to these transcripts or by secondary downstream regulation. Based on previous findings that miRs can regulate sets of genes functionally connected within a single pathway [48, 49], we employed a KEGG (Kyoto Encyclopedia of Genes and Genomes) analysis to map altered miR-338 mediated transcripts into distinct gene pathways. This inquiry identified several enriched canonical pathways as summarized in Fig. 4d. Among the putative miR-338 mediated gene pathways identified, the axon guidance pathway was found to be the most significant with a calculated p value of 4.40E-4, containing 17 up- or downregulated axon guidance genes. To further identify direct miR-338 targets within this pathway, we filtered out the eight (of the total of 17) significantly upregulated axon guidance genes as a consequence of miR-338 inhibition (Fig. 4e). To further define miR-338 regulated transcripts, the computational miR seed prediction algorithm DIANA-microT v5.0 was utilized to identify putative miR-338 binding sites within the eight axon guidance genes. A cut-off threshold of at least 0.6 or higher was used, where a higher score means a lower amount of false positives [50]. Furthermore, the identified binding sites needed to be conserved between mouse and rat. This analysis resulted in the identification of one binding site within the 3′ UTR of *Robo2* and two binding sites in *Rock2* (Rho-associated protein kinase 2) (Fig. 4e). qPCR validation confirmed the upregulation of all of the selected axon guidance genes (control vs., *Pak6* $p=0.0046$, *Robo2* $p=<0.0001$, *Ucn5c* $p=0.0002$, *Ablim3* $p=0.002$, *Rock2* $p=<0.0001$, *Ngef* $p=0.002$ and *Pak1* $p=0.0046$) identified by RNA sequencing (Fig. 4f). These results suggest that miR-338 has the capacity to alter the expression of several axon guidance genes either by directly or indirectly interacting with downstream target transcripts.

miR-338 Regulates Robo2 Gene Expression

To further pinpoint miR-338 targets responsible for the miR-338 induced neurodevelopmental phenotypes, we set out to identify consensus miR-338 regulatory sequences within the 3′ UTRs of the RNA sequencing determined putative target genes. Although initial luciferase reporter assays revealed that the 3′ UTR of *Rock2* is not directly regulated by miR-338 (data not shown), we further examined *Robo2* as a potential direct miR-338 target since it contains a conserved miR-338 binding site within its 3′ UTR (Fig. 5a) and its mRNA levels were upregulated in miR-338 repressed cortical cells, as identified by RNA sequencing and qPCR (Fig. 4e, f). In order to pinpoint miR-338 regulation sites within the 3′ UTR of *Robo2*, we performed luciferase gene activity assays using a luciferase vector carrying the 3′ UTR of *Robo2* containing the putative miR-338 binding site. The *Robo2* 3′ UTR luciferase reporter construct was co-transfected with a miR-338 mimic or a NT control into HEK cells to assess whether increased miR-338 levels result in decreased luciferase activity. Adding the 3′ UTR of *Robo2* led to a significant 24 % decrease in luciferase activity compared to NT-transfected control (*Robo2* 3′ UTR NT control vs. miR-338 mimic, $p=<0.0001$) (Fig. 4b). Furthermore, miR-338 inhibition by transfection of anti-miR-338 inhibitor caused an increase of 13 % (NT control vs. anti-miR-338 30 nM, $p=<0.0001$) and 40 % (NT control vs. anti-miR-338 60 nM, $p=<0.0001$) in luciferase activity in a dose-dependent manner as compared to the NT-transfected control (Fig. 5b). To show that this modulation by miR-338 is due to direct association with the binding site residing in the 3′ UTR of *Robo2*, we generated a luciferase reporter construct in which the 7-mer seed sequence for miR-338 was entirely deleted. This mutation abolished miR-338-induced regulation both during overexpression and inhibition of miR-338 (Fig. 5b), showing that miR-338 can directly bind to the 3′ UTR of *Robo2* and that the seed sequence located at nucleotide positions 542–548 is essential for regulation to take place. To examine whether miR-338 can regulate *Robo2* mRNA levels, primary cortical neurons were transfected with 50 nM miR-338 mimic or 50 nM anti-miR-338 inhibitor at DIV 2 followed by RNA isolation at DIV6 and subsequently qPCR analysed. This analysis revealed a bidirectional regulation of *Robo2* during miR-338 modulation (Fig. 5c). Overexpression of miR-338 resulted in a significant decrease of 28 % in *Robo2* mRNA levels, compared to a NT-transfected control (NT control vs. miR-338 mimic, $p=0.0106$), while inhibition of miR-338 led to a significant 40 % increase in *Robo2* mRNA levels (NT control vs. anti-miR-338, $p=0.0023$). This outcome indicates that miR-338 regulation of *Robo2* is due to mRNA destabilization resulting in the degradation of the transcript. To investigate whether the effect of this regulation is also detectable at the protein level, protein samples were extracted from DIV 6 primary cortical cells either overexpressing or underexpressing miR-338 (transfected at DIV 2). As expected, a bidirectional regulation was observed with a 27 % decrease (NT control vs. miR-338 mimic, $p=0.0037$) and 48 % increase (NT control vs. anti-miR-338, $p=0.0003$) in Robo2 protein during miR-338 overexpression and inhibition compared to the control, respectively (Fig. 5d). To further examine the regulation of *Robo2* by miR-338, we asked whether gain- or loss-of-function of miR-338 could modulate Robo2 protein expression. To study this, we utilized the same protocol used in the experiments described above where DIV 6 cortical cells were transfected with an NT control, miR-338 mimic or anti-miR-338 inhibitor, followed by fluorescently labelling Robo2 protein. Overexpression of miR-338 resulted in a significant 26 % decrease (NT control vs. miR-338 mimic, $p=0.0146$), while inhibition of miR-338 led to a 32 % increase of Robo2 protein (NT control vs. anti-miR-338, $p=0.015$) (Fig. 5d). In

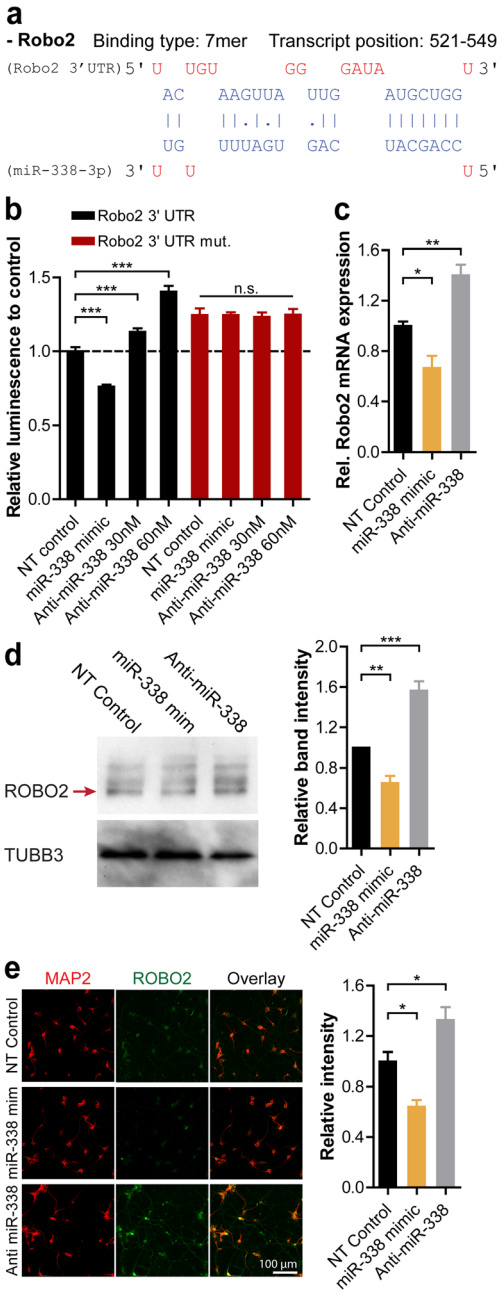

◀ **Fig. 5** miR-338 regulates Robo2. **a** In silico identified miR-338-3p-binding site in the 3′ UTR of *Robo2* conserved in mouse and rat. Both the type of seed sequence binding and the nucleotide position within the 3′ UTR are shown. Nucleotides depicted in blue are complementary (connected with a blue line), while nucleotides in red are not complementary to miR-338-3p. Nucleotides forming a wobble base pair are connected with a blue dot. **b** HEK-293T cells transfected with luciferase reporter constructs containing the 3′ UTR fragment of *Robo2* (black bars), in which overexpression led to a decrease, while a dose-dependent inhibition of miR-338 increases the luciferase activity compared to the NT control (*dotted black line*). A miR-338 seed mutant (*red bars*) did not respond to miR-338 modulation. $n = 4$ independent experiments with 4–8 samples per repetition. **c**–**e** Cortical neurons were transfected with 50 mM NT control, miR-338 mimic or an anti-miR-338 at DIV 2 and analysed at DIV 6. **b** Relative *Robo2* mRNA levels in cortical neurons assessed by qPCR during miR-338 overexpression and inhibition, compared to a NT control. $n = 4$ samples from independent experiments. **c** Immunoblot of Robo2 protein of samples isolated from cortical neurons transfected with NT control, miR-338 mimic or anti-miR-338 with its corresponding band intensity quantification. For Robo2, the intensity of the lower ~150 kDa band was measured, indicated with the red arrow. TUBB3 (tubulin, beta 3 class III) served as loading control. $n = 3$ samples from independent experiments. **d** Immunostaining of MAP2 (*red*), Robo2 (*green*) and the overlay in primary cortical neurons transfected with NT control, miR-338 mimic and anti-miR-338. Average cell intensities collected from $n = 3$ samples from independent experiments. Data represents mean fold change with *error bars* ± s.e.m. One-way ANOVA with Bonferroni multiple comparison test; $*p < 0.05$, $**p < 0.01$, $***p < 0.001$

conclusion, these data show that miR-338 targets the 3′ UTR of *Robo2* and post-transcriptionally regulates its expression in cortical neurons.

Discussion

This study provides evidence that miR-388 is important for dendrite formation and axon outgrowth during cortical neuronal development. The dendrites of cultured cortical neurons were significantly less complex when miR-338 activity was inhibited, while the length and diameter of the dendritic spines were increased. Furthermore, miR-338 inhibition in cortical neurons resulted in longer axons, while increasing miR-338 levels reduced axon growth. In addition, whole-transcriptome analysis of cultured cortical neurons in which miR-338 activity was inhibited identified a large set of upregulated transcripts involved in neuronal development. Pathway-based gene clustering pointed towards a significant enrichment of axon guidance genes, of which we found *Robo2* to be a direct miR-338 target. Together, our observations support the idea that manipulating miR-338 expression levels induces changes in neurite outgrowth of cortical neurons, suggesting that this miR actively participates in the promotion of neuronal development.

We assessed the underlying mechanism of miR-338 regulation in neuronal cortical development by identifying its target genes. This approach provided a global view of alterations to the transcriptome during miR-338 inhibition. Our studies suggest that miR-338 is involved in the post-transcriptional regulation of neurite growth by steering cortical neurons towards dendritic growth while decreasing axon growth. Indeed, our analysis of miR-338 targets identified a large number of genes involved in axon or dendrite growth and development pathways. In keeping with these findings, we have previously demonstrated that miR-338 is involved in controlling axonal outgrowth in sympathetic neurons by regulating the local levels of a number of nuclear-encoded mitochondrial proteins in the axons, such as COXIV and ATP5G1 [21, 27]. Moreover, we have shown that in rat hippocampal

neurons, miR-338 can directly target the 3′ UTR of its host gene, encoding *AATK* [34], a kinase that plays a critical role in neuronal differentiation and axon outgrowth [23, 24]. However, the capacity of miR-338 to destabilize AATK mRNA in cortical cells at early developmental stages was not confirmed using transcriptome analysis of cortical neurons. This confound could be due to the different cell types or AATK regulation of miR-338 could be mediated at a different neurodevelopmental stage. The study presented here suggests that miR-338's action to modulate neuronal outgrowth and differentiation is mediated by direct and indirect regulation of several axonal guidance pathway genes, such as *Robo2*, since miR-338 overexpression results in *Robo2* mRNA degradation and its subsequent translational diminution.

Previously, Robo2 has been identified as a receptor important in stimulating axon growth [51]. Furthermore, Robo2 knock-out studies have shown exacerbated neuronal progenitor cell division and enhanced neuronal migration towards the cortical plate, as well as an increase in the outgrowth of neurite processes of migrating neurons [52, 53]. These findings are largely in line with the observed effect of miR-338 on process growth and branching, and may at least be partly attributed to the modulation of *Robo2* levels. This and other studies suggest that miR-338 has multiple downstream targets with converging roles in neural growth and development. Furthermore, it has also become increasingly clear that miRs can modulate gene expression in an indirect manner [54, 55]. This non-canonical gene regulation could be facilitated by directly regulating the expression of transcription factors, RNA binding molecules, components of the nonsense-mediated mRNA decay pathway or modulate the activity of the RNA translation system [54, 56, 57]. In light of this, we predict that direct and indirect regulation of axon guidance genes, including *Robo2*, contribute to miR-338's guided control of cortical development.

Accumulating evidence indicates that post-transcriptional mechanisms involving miRs are essential for the regulation of cortical development. Our data demonstrate a critical role of miR-338 during neurite development of cortical neurons, and further supports the notion for a tight temporal regulation of this miR's expression for proper function in this process. Nevertheless, due to the extensive expression of miR-338 throughout the development of cortical cells, we suspect that miR-338 modulates gene expression at multiple steps of cortical development, which could be indicative of a multitude of neurodevelopmental functions for this miR.

The miR-338 target *Robo2* is cooperatively involved with other axon guidance genes in axon development and could be responsible for the observed miR-338 cellular phenotypes. However, additional direct and indirect targets of miR-388 are likely to contribute as well. Indeed, miR-338 inhibition resulted in the altered expression of a relatively large number of axon guidance genes. This emphasizes the need to delineate the significance of the full spectrum of genes regulated by miR-338 at a particular time and place in order to understand how these targets collectively contribute to the assigned function of miR-338 in cortical neuronal development.

Acknowledgments We thank N van Bakel, D Versteegden and M van Kessel for technical assistance. We thank the RIMLS microscopy platform (http://ncmls.nl/technology-platform/microscope-imaging-centre/) for support and maintenance of the equipment. The research of the authors is supported by grants from the "Donders Center for Neuroscience fellowship award of the Radboudumc" [to A. A.]; the "FP7-Marie Curie International Reintegration Grant" [to A. A. grant number 276868] and GENCODYS, an EU FP7 large-scale integrating project grant [Grant number 241995] [to HvB].

Compliance with Ethical Standards All animal use, care and experiments were performed according to protocols approved by the Committee for Animal Experiments of the Radboud University Nijmegen Medical Centre, Nijmegen, The Netherlands.

Conflict of Interest The authors declare no competing financial interests.

References

1. Corbett MA, Bahlo M, Jolly L, Afawi Z, Gardner AE, Oliver KL, Tan S, Coffey A et al (2010) A focal epilepsy and intellectual disability syndrome is due to a mutation in TBC1D24. Am J Hum Genet 87(3):371–375. doi:10.1016/j.ajhg.2010.08.001
2. Guerrini R, Sicca F, Parmeggiani L (2003) Epilepsy and malformations of the cerebral cortex. Epileptic Disord: Int Epilepsy J Videotape 5(Suppl 2):S9–S26
3. Levitt P, Eagleson KL, Powell EM (2004) Regulation of neocortical interneuron development and the implications for neurodevelopmental disorders. Trends Neurosci 27(7):400–406. doi:10.1016/j.tins.2004.05.008
4. Schmidt MJ, Mirnics K (2015) Neurodevelopment, GABA system dysfunction, and schizophrenia. Neuropsychopharmacol: Off Publ Am Coll Neuropsychopharmacol 40(1):190–206. doi:10.1038/npp.2014.95
5. Schubert D, Martens GJ, Kolk SM (2015) Molecular underpinnings of prefrontal cortex development in rodents provide insights into the etiology of neurodevelopmental disorders. Mol Psychiatry 20(7):795–809. doi:10.1038/mp.2014.147
6. Lui JH, Hansen DV, Kriegstein AR (2011) Development and evolution of the human neocortex. Cell 146(1):18–36. doi:10.1016/j.cell.2011.06.030
7. Lim LP, Lau NC, Garrett-Engele P, Grimson A, Schelter JM, Castle J, Bartel DP, Linsley PS et al (2005) Microarray analysis shows that some microRNAs downregulate large numbers of target mRNAs. Nature 433(7027):769–773. doi:10.1038/nature03315
8. Stark A, Brennecke J, Bushati N, Russell RB, Cohen SM (2005) Animal MicroRNAs confer robustness to gene expression and have a significant impact on 3′UTR evolution. Cell 123(6):1133–1146. doi:10.1016/j.cell.2005.11.023
9. Li X, Cassidy JJ, Reinke CA, Fischboeck S, Carthew RW (2009) A microRNA imparts robustness against environmental fluctuation during development. Cell 137(2):273–282. doi:10.1016/j.cell.2009.01.058

10. Ebert MS, Sharp PA (2012) Roles for microRNAs in conferring robustness to biological processes. Cell 149(3):515–524. doi:10.1016/j.cell.2012.04.005
11. Rago L, Beattie R, Taylor V, Winter J (2014) miR379-410 cluster miRNAs regulate neurogenesis and neuronal migration by fine-tuning N-cadherin. EMBO J 33(8):906–920. doi:10.1002/embj.201386591
12. Gaughwin P, Ciesla M, Yang H, Lim B, Brundin P (2011) Stage-specific modulation of cortical neuronal development by Mmu-miR-134. Cereb Cortex 21(8):1857–1869. doi:10.1093/cercor/bhq262
13. Dajas-Bailador F, Bonev B, Garcez P, Stanley P, Guillemot F, Papalopulu N (2012) microRNA-9 regulates axon extension and branching by targeting Map1b in mouse cortical neurons. Nature neuroscience. doi:10.1038/nn.3082
14. Smrt RD, Szulwach KE, Pfeiffer RL, Li X, Guo W, Pathania M, Teng ZQ, Luo Y et al (2010) MicroRNA miR-137 regulates neuronal maturation by targeting ubiquitin ligase mind bomb-1. Stem Cells 28(6):1060–1070. doi:10.1002/stem.431
15. Schratt GM, Tuebing F, Nigh EA, Kane CG, Sabatini ME, Kiebler M, Greenberg ME (2006) A brain-specific microRNA regulates dendritic spine development. Nature 439(7074):283–289. doi:10.1038/nature04367
16. Mellios N, Sugihara H, Castro J, Banerjee A, Le C, Kumar A, Crawford B, Strathmann J et al (2011) miR-132, an experience-dependent microRNA, is essential for visual cortex plasticity. Nat Neurosci 14(10):1240–1242. doi:10.1038/nn.2909
17. Lee K, Kim JH, Kwon OB, An K, Ryu J, Cho K, Suh YH, Kim HS (2012) An activity-regulated microRNA, miR-188, controls dendritic plasticity and synaptic transmission by downregulating neuropilin-2. J Neurosci: Off J Soc Neurosci 32(16):5678–5687. doi:10.1523/JNEUROSCI.6471-11.2012
18. Im HI, Kenny PJ (2012) MicroRNAs in neuronal function and dysfunction. Trends Neurosci 35(5):325–334. doi:10.1016/j.tins.2012.01.004
19. Beveridge NJ, Gardiner E, Carroll AP, Tooney PA, Cairns MJ (2010) Schizophrenia is associated with an increase in cortical microRNA biogenesis. Mol Psychiatry 15(12):1176–1189. doi:10.1038/mp.2009.84
20. Perkins DO, Jeffries CD, Jarskog LF, Thomson JM, Woods K, Newman MA, Parker JS, Jin J et al (2007) microRNA expression in the prefrontal cortex of individuals with schizophrenia and schizoaffective disorder. Genome Biol 8(2):R27. doi:10.1186/gb-2007-8-2-r27
21. Aschrafi A, Kar AN, Natera-Naranjo O, Macgibeny MA, Gioio AE, Kaplan BB (2012) MicroRNA-338 regulates the axonal expression of multiple nuclear-encoded mitochondrial mRNAs encoding subunits of the oxidative phosphorylation machinery. Cell Mol Life Sci: CMLS. doi:10.1007/s00018-012-1064-8
22. Zhao X, He X, Han X, Yu Y, Ye F, Chen Y, Hoang T, Xu X et al (2010) MicroRNA-mediated control of oligodendrocyte differentiation. Neuron 65(5):612–626. doi:10.1016/j.neuron.2010.02.018
23. Raghunath M, Patti R, Bannerman P, Lee CM, Baker S, Sutton LN, Phillips PC, Damodar Reddy C (2000) A novel kinase, AATYK induces and promotes neuronal differentiation in a human neuroblastoma (SH-SY5Y) cell line. Brain Res Mol Brain Res 77(2):151–162
24. Takano T, Tomomura M, Yoshioka N, Tsutsumi K, Terasawa Y, Saito T, Kawano H, Kamiguchi H et al (2012) LMTK1/AATYK1 is a novel regulator of axonal outgrowth that acts via Rab11 in a Cdk5-dependent manner. J Neurosci: Off J Soc Neurosci 32(19):6587–6599. doi:10.1523/JNEUROSCI.5317-11.2012
25. Takano T, Urushibara T, Yoshioka N, Saito T, Fukuda M, Tomomura M, Hisanaga S (2014) LMTK1 regulates dendritic formation by regulating movement of Rab11A-positive endosomes. Mol Biol Cell 25(11):1755–1768. doi:10.1091/mbc.E14-01-0675
26. Natera-Naranjo O, Aschrafi A, Gioio AE, Kaplan BB (2010) Identification and quantitative analyses of microRNAs located in the distal axons of sympathetic neurons. RNA 16(8):1516–1529. doi:10.1261/rna.1833310
27. Aschrafi A, Schwechter AD, Mameza MG, Natera-Naranjo O, Gioio AE, Kaplan BB (2008) MicroRNA-338 regulates local cytochrome c oxidase IV mRNA levels and oxidative phosphorylation in the axons of sympathetic neurons. J Neurosci: Off J Soc Neurosci 28(47):12581–12590. doi:10.1523/JNEUROSCI.3338-08.2008
28. De Felice B, Annunziata A, Fiorentino G, Borra M, Biffali E, Coppola C, Cotrufo R, Brettschneider J et al (2014) miR-338-3p is over-expressed in blood, CFS, serum and spinal cord from sporadic amyotrophic lateral sclerosis patients. Neurogenetics 15(4):243–253. doi:10.1007/s10048-014-0420-2
29. Ragusa M, Majorana A, Banelli B, Barbagallo D, Statello L, Casciano I, Guglielmino MR, Duro LR et al (2010) MIR152, MIR200B, and MIR338, human positional and functional neuroblastoma candidates, are involved in neuroblast differentiation and apoptosis. J Mol Med 88(10):1041–1053. doi:10.1007/s00109-010-0643-0
30. He M, Liu Y, Wang X, Zhang MQ, Hannon GJ, Huang ZJ (2012) Cell-type-based analysis of microRNA profiles in the mouse brain. Neuron 73(1):35–48. doi:10.1016/j.neuron.2011.11.010
31. Lin Q, Wei W, Coelho CM, Li X, Baker-Andresen D, Dudley K, Ratnu VS, Boskovic Z et al (2011) The brain-specific microRNA miR-128b regulates the formation of fear-extinction memory. Nat Neurosci 14(9):1115–1117. doi:10.1038/nn.2891
32. Meister G, Landthaler M, Patkaniowska A, Dorsett Y, Teng G, Tuschl T (2004) Human Argonaute2 mediates RNA cleavage targeted by miRNAs and siRNAs. Mol Cell 15(2):185–197. doi:10.1016/j.molcel.2004.07.007
33. Zhang F, Gradinaru V, Adamantidis AR, Durand R, Airan RD, de Lecea L, Deisseroth K (2010) Optogenetic interrogation of neural circuits: technology for probing mammalian brain structures. Nat Protoc 5(3):439–456. doi:10.1038/nprot.2009.226
34. Kos A, Olde Loohuis NF, Wieczorek ML, Glennon JC, Martens GJ, Kolk SM, Aschrafi A (2012) A potential regulatory role for intronic microRNA-338-3p for its host gene encoding apoptosis-associated tyrosine kinase. PLoS One 7(2):e31022. doi:10.1371/journal.pone.0031022
35. Vandesompele J, De Preter K, Pattyn F, Poppe B, Van Roy N, De Paepe A, Speleman F (2002) Accurate normalization of real-time quantitative RT-PCR data by geometric averaging of multiple internal control genes. Genome Biol 3(7):0034
36. Nonne N, Ameyar-Zazoua M, Souidi M, Harel-Bellan A (2010) Tandem affinity purification of miRNA target mRNAs (TAP-Tar). Nucleic Acids Res 38(4):e20. doi:10.1093/nar/gkp1100
37. da Huang W, Sherman BT, Lempicki RA (2009) Systematic and integrative analysis of large gene lists using DAVID bioinformatics resources. Nat Protoc 4(1):44–57. doi:10.1038/nprot.2008.211
38. da Huang W, Sherman BT, Lempicki RA (2009) Bioinformatics enrichment tools: paths toward the comprehensive functional analysis of large gene lists. Nucleic Acids Res 37(1):1–13. doi:10.1093/nar/gkn923
39. Maragkakis M, Reczko M, Simossis VA, Alexiou P, Papadopoulos GL, Dalamagas T, Giannopoulos G, Goumas G et al (2009) DIANA-microT web server: elucidating microRNA functions through target prediction. Nucleic Acids Res 37(Web Server issue):W273–W276. doi:10.1093/nar/gkp292
40. Meijering E, Jacob M, Sarria JC, Steiner P, Hirling H, Unser M (2004) Design and validation of a tool for neurite tracing and analysis in fluorescence microscopy images. Cytom Part A: J Int Soc Anal Cytol 58(2):167–176. doi:10.1002/cyto.a.20022
41. Rodriguez A, Ehlenberger DB, Dickstein DL, Hof PR, Wearne SL (2008) Automated three-dimensional detection and shape

classification of dendritic spines from fluorescence microscopy images. PLoS One 3(4):e1997. doi:10.1371/journal.pone.0001997
42. Ebert MS, Neilson JR, Sharp PA (2007) MicroRNA sponges: competitive inhibitors of small RNAs in mammalian cells. Nat Methods 4(9):721–726. doi:10.1038/Nmeth1079
43. Nikolic M, Dudek H, Kwon YT, Ramos YFM, Tsai LH (1996) The cdk5/p35 kinase is essential for neurite outgrowth during neuronal differentiation. Gene Dev 10(7):816–825. doi:10.1101/Gad.10.7.816
44. Aschrafi A, Natera-Naranjo O, Gioio AE, Kaplan BB (2010) Regulation of axonal trafficking of cytochrome c oxidase IV mRNA. Mol Cell Neurosci 43(4):422–430. doi:10.1016/j.mcn.2010.01.009
45. Ambros V (2004) The functions of animal microRNAs. Nature 431(7006):350–355. doi:10.1038/nature02871
46. Martinez NJ, Gregory RI (2010) MicroRNA gene regulatory pathways in the establishment and maintenance of ESC identity. Cell Stem Cell 7(1):31–35. doi:10.1016/j.stem.2010.06.011
47. Eichhorn SW, Guo H, McGeary SE, Rodriguez-Mias RA, Shin C, Baek D, Hsu SH, Ghoshal K et al (2014) mRNA destabilization is the dominant effect of mammalian microRNAs by the time substantial repression ensues. Mol Cell 56(1):104–115. doi:10.1016/j.molcel.2014.08.028
48. Inui M, Martello G, Piccolo S (2010) MicroRNA control of signal transduction. Nat Rev Mol Cell Biol 11(4):252–263. doi:10.1038/nrm2868
49. Ghosh T, Aprea J, Nardelli J, Engel H, Selinger C, Mombereau C, Lemonnier T, Moutkine I et al (2014) MicroRNAs establish robustness and adaptability of a critical gene network to regulate progenitor fate decisions during cortical neurogenesis. Cell Rep 7(6):1779–1788. doi:10.1016/j.celrep.2014.05.029
50. Maragkakis M, Alexiou P, Papadopoulos GL, Reczko M, Dalamagas T, Giannopoulos G, Goumas G, Koukis E et al (2009) Accurate microRNA target prediction correlates with protein repression levels. BMC Bioinforma 10:295. doi:10.1186/1471-2105-10-295
51. Hivert B, Liu Z, Chuang CY, Doherty P, Sundaresan V (2002) Robo1 and Robo2 are homophilic binding molecules that promote axonal growth. Mol Cell Neurosci 21(4):534–545
52. Borrell V, Cardenas A, Ciceri G, Galceran J, Flames N, Pla R, Nobrega-Pereira S, Garcia-Frigola C et al (2012) Slit/Robo signaling modulates the proliferation of central nervous system progenitors. Neuron 76(2):338–352. doi:10.1016/j.neuron.2012.08.003
53. Andrews W, Barber M, Hernadez-Miranda LR, Xian J, Rakic S, Sundaresan V, Rabbitts TH, Pannell R et al (2008) The role of Slit-Robo signaling in the generation, migration and morphological differentiation of cortical interneurons. Dev Biol 313(2):648–658. doi:10.1016/j.ydbio.2007.10.052
54. Helwak A, Kudla G, Dudnakova T, Tollervey D (2013) Mapping the human miRNA interactome by CLASH reveals frequent noncanonical binding. Cell 153(3):654–665. doi:10.1016/j.cell.2013.03.043
55. Wang WX, Wilfred BR, Xie K, Jennings MH, Hu YH, Stromberg AJ, Nelson PT (2010) Individual microRNAs (miRNAs) display distinct mRNA targeting "rules". RNA Biol 7(3):373–380
56. Grueter CE, van Rooij E, Johnson BA, DeLeon SM, Sutherland LB, Qi X, Gautron L, Elmquist JK et al (2012) A cardiac microRNA governs systemic energy homeostasis by regulation of MED13. Cell 149(3):671–683. doi:10.1016/j.cell.2012.03.029
57. Bruno IG, Karam R, Huang L, Bhardwaj A, Lou CH, Shum EY, Song HW, Corbett MA et al (2011) Identification of a microRNA that activates gene expression by repressing nonsense-mediated RNA decay. Mol Cell 42(4):500–510. doi:10.1016/j.molcel.2011.04.018